CRYSTAL GROWTH & DESIGN

pubs.acs.org/crystal

Article

1-Ethyluracil, a New Scaffold for Preparing Multicomponent Forms: Synthesis, Characterization, and Computational Studies

Yannick Roselló, Mónica Benito, Miquel Barceló-Oliver, Antonio Frontera,* and Elies Molins*

Cite This: *Cryst. Growth Des.* 2021, 21, 4857−4870

Read Online

ACCESS | Metrics & More | Article Recommendations | Supporting Information

ABSTRACT: In this work, we describe the successful preparation of a series of cocrystals of the modified nucleobase 1-ethyluracil with different coformers in a 1:1 or 2:1 (nucleobase:coformer) ratio including urea (URE) or some compounds containing carboxylic and hydroxyl groups such as L-malic acid (MAL), L-tartaric acid (TAR), 2-hydroxybenzoic acid (SAL), 4-hydroxybenzoic acid (4HB), and 2,4-dihydroxybenzoic acid (DHB). The influence of the hydroxyl substituent on the alkyl chain for **1·TAR** and **1·SAL** cocrystals or the phenyl ring for **1·SAL**, **1·4HB**, and **1·DHB** multicomponent solids was studied. All of the compounds were characterized by powder X-ray diffraction, FT-IR, and thermal methods. Moreover, for those whose single-crystal structures could be determined, computational studies were also performed to investigate the factors that may affect the cocrystal formation, the recurrent motifs, and the energies associated with the H-bonding interactions using DFT calculations and a combination of the quantum theory of atoms in molecules (QTAIM) and the noncovalent interaction index (NCIplot) computational tools.

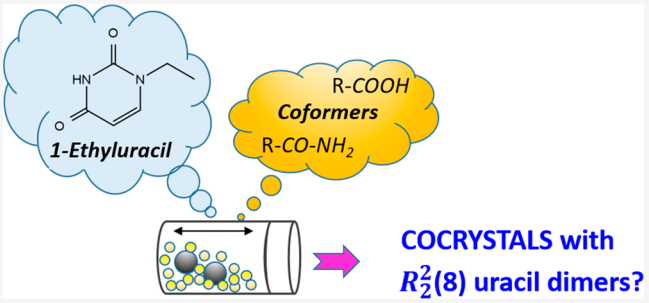

INTRODUCTION

In recent years, crystal engineering has emerged as a predictive tool for studying and understanding the arrangement of molecules, giving birth to different solid materials with modified physicochemical properties and performances.[1,2] Especially in the pharmaceutical industry but also in other areas such as energetic materials, the objective has been to overcome undesirable properties (chemical instability, low solubility, hygroscopicity, untableting, ...) before the commercialization of drugs or to ameliorate the viability of the available explosives.[3,4] Although traditionally polymorphic and salt screenings have been the selected methods for exploring these versatile solid materials, more recently cocrystals have re-emerged as useful alternatives.[5,6] Cocrystals are defined as multicomponent solids in which individual molecules are held together by noncovalent interactions, often hydrogen bonds as well as halogen bonding,[7−10] and $\pi-\pi$ stacking interactions. As reviewed recently, thanks to the effort done by academic and industry researchers in finding new solid forms/cocrystals, a few pharmaceutical cocrystals have been approved and commercialized.[11]

Nonetheless, not just active pharmaceutical ingredients and energetic materials have been studied from a crystal engineering point of view. Biomolecules such as nucleobases have also attracted interest, first because their base-pairing nature in the solid state could be correlated to natural DNA or RNA.[12] Second, they are well recognized as integral components of a great number of pharmaceuticals mostly having antiviral and/or antitumoral activity as well as acting as antibacterial, antiparasitic, or vasodilator/antihypertensive compounds. Recently, istradefylline has been FDA approved for Parkinson's disease in adults.[13−17]

Among the nucleobases, uracil and its derivatives contain N−H and C=O groups, which are suitable hydrogen-bonding donors and acceptors, respectively, and could result in strong hydrogen-bonded synthons.[6] Up to now, several uracil derivatives have also been described for cocrystallization with other nucleobases[18−21] or with several small molecules used as coformers. This is the case for the modified uracils: 6-chlorouracil and 6-chloro-3-methyluracil,[22] 6-methyl-2-thiouracil,[23] orotic and isoorotic acids,[24] and the well-known antineoplastic agent 5-fluorouracil[5,25−31] and its analogue, tegafur.[32]

In this paper, we explore the ability of 1-ethyluracil (**1**), a modified uracil with a N−H group blocked as observed in many other known APIs (such as 5-fluoro-1-propargyluracil, idoxuridine, telbivudine, floxuridine, carmofur, ...), as a new scaffold for cocrystallization by liquid-assisted grinding (LAG) and solvent crystallization. The molecular structures of 1-ethyluracil and the coformers selected in our study are depicted in Scheme 1.

Received: February 15, 2021
Revised: July 21, 2021
Published: August 3, 2021

https://doi.org/10.1021/acs.cgd.1c00175
Cryst. Growth Des. 2021, 21, 4857−4870

Scheme 1. Molecular Structures of 1-Ethyluracil and Selected Coformers Used in This Work

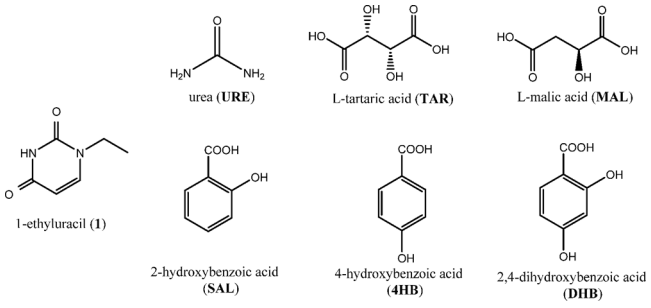

The selected coformers include urea, the two aliphatic carboxylic acids L-tartaric acid and L-malic acid, and several monohydroxyl- and dihydroxyl-substituted benzoic acids. All of them are categorized as GRAS/EAFUS (generally recognized as safe/everything added to food in the United States) molecules.[33] For instance, the presence of malic and tartaric acids is very common in some fruits (pears, bananas, apples, and grapes). 2-Hydroxybenzoic acid, also known as salicylic acid, is a recognized drug used for aches and pain treatment, and its structural isomer, 4-hydroxybenzoic acid, is used as a flavoring or adjuvant agent and has antioxidant properties.[34]

EXPERIMENTAL METHODS

All reagents were purchased from Sigma-Aldrich Co. Analytical-grade solvents were used for the crystallization experiments.

Synthesis of 1-Ethyluracil (1). The modified uracil was obtained following a synthesis described previously.[35] Briefly, the synthesis of 1-ethyluracil was carried out in two steps. In the first step, the silylation of carbonyl groups of uracil was afforded as follows. Hexamethyldisilazane (HDMS, 200 mL, 950 mmol, d = 0.774 g mL^{-1}) and uracil (11.208 g, 100 mmol) were mixed in the presence of catalytic amounts of ammonium sulfate under a nitrogen atmosphere. The mixture was stirred under reflux for 4 h. Then the excess HDMS was distilled. The remaining product was stored under nitrogen. The second step includes substitution of silylated units by ethyl groups. O,O'-Bis(trimethylsilyl)-uracil (15 mmol), α-bromoethane (15 mmol), and anhydrous acetonitrile (30 mL) were mixed in a 45 mL Parr digestion vessel. The mixture was placed in an oven at 130 °C for 36 h. The resulting product was first washed with boiling methanol (50 mL) for 30 min to eliminate residual bromide and then concentrated in a rotary evaporator to allow precipitation of fine white needles. The purity of the solid was confirmed by proton NMR.

^{1}H NMR (DMSO-d_6, 300 MHz) δ, ppm: 11.17 (1 H, s, N(3)-H), 7.63 (1 H, d, H(6), J = 7.8 Hz), 5.51 (1 H, dd, H(5), J = 7.8 and 2.4 Hz), 3.65 (2 H, q, H(7), J = 7.1 Hz), 1.12 (3 H, t, H(8), J = 7.0 Hz).

Screening by Grinding. The mechanochemical synthesis of cocrystals was performed by using a Retsch MM400 ball mixer in 10 mL agate grinding jars with two 5 mm agate balls. 1-Ethyluracil and the selected coformer in a 1:1 or 2:1 stoichiometric molar ratio were ground with two drops of solvent for 30 min at 30 Hz.

Synthesis of 1-Ethyluracil−Urea (1·URE). A mixture of 1-ethyluracil (100.12 mg, 0.714 mmol) and urea (43.43 mg, 0.723 mmol) was placed in a grinding jar with two drops of distilled water or methanol. The mixture was milled for 30 min. Single crystals were obtained in nitromethane with a few drops of ethanol.

Synthesis of 1-Ethyluracil−L-Malic Acid Cocrystal (1·MAL). A mixture of 1-ethyluracil (100.07 mg, 0.714 mmol) and L-malic acid (47.87 mg, 0.357 mmol) was placed in a grinding jar with two drops of nitromethane. The mixture was milled for 30 min. Single crystals were obtained by dissolution of the solid in nitromethane by heating. The solution was cooled to room temperature, and suitable crystals were obtained after a couple of days.

Synthesis of 1-Ethyluracil−L-Tartaric Acid (1·TAR). A mixture of 1-ethyluracil (100.66 mg, 0.718 mmol) and L-tartaric acid (53.59 mg, 0.357 mmol) was placed in a grinding jar with two drops of distilled water. The mixture was milled for 30 min. Suitable single crystals were obtained by dissolving the product in ethanol and using cyclohexane as an antisolvent by vapor diffusion evaporation.

Synthesis of 1-Ethyluracil−2-Hydroxybenzoic Acid or Salicylic Acid Cocrystal (1·SAL). A mixture of 1-ethyluracil (100.19 mg, 0.715 mmol) and salicylic acid (99.35 mg, 0.719 mmol) was placed in a grinding jar with two drops of methanol. The mixture was milled for 30 min. Suitable crystals were afforded by dissolving the product in a water−methanol mixture (1:1) and filtering the solution allowing it to evaporate at room temperature.

Synthesis of 1-Ethyluracil−4-Hydroxybenzoic Acid Hydrated Cocrystal (1·4HB·H$_2$O). A mixture of 1-ethyluracil (75 mg, 0.535 mmol) and 4-hydroxybenzoic acid (73.97 mg, 0.536 mmol) was placed in a grinding jar with two drops of distilled water. The mixture was milled for 30 min. From slow evaporation of a water−ethanol solution of the previous solid, single crystals of **4HB·H$_2$O** were obtained.

Synthesis of 1-Ethyluracil−4-Hydroxybenzoic Acid Cocrystal (1·4HB_FI). 1·4HB·H$_2$O was dried at 50 °C under vacuum for 4 h.

Synthesis of 1-Ethyluracil−4-Hydroxybenzoic Acid Cocrystal (1·4HB_FII). A mixture of 1-ethyluracil (75.14 mg, 0.536 mmol) and 4-hydroxybenzoic acid (74.10 mg, 0.536 mmol) was placed in a grinding jar with two drops of methanol. The mixture was milled for 30 min. Single crystals were obtained from a mixture of acetonitrile and propyl acetate by slow evaporation.

1-Ethyluracil (75.10 mg, 0.536 mmol) and 4-hydroxybenzoic acid (74.06 mg, 0.536) were dissolved in methanol (1 mL) at room temperature. The solution was filtered using a 0.20 μm Nylon syringe filter and allowed to slowly evaporate at room temperature. The resulting solid was smoothly ground to obtain a fine powder.

Synthesis of 1-Ethyluracil−2,4-Dihydroxybenzoic Acid Cocrystal (1·DHB). A mixture of 1-ethyluracil (99.97 mg, 0.713 mmol) and 2,4-dihydroxybenzoic acid (110.18 mg, 0.715 mmol) was placed in a grinding jar with two drops of distilled water. The mixture was milled for 30 min. Single crystals were obtained by dissolving the product in a water−methanol mixture (1:1) and filtering and slowly evaporating the solution at room temperature.

Stability Study. The solids **1·4HB_FI** and **1·4HB_FII** were stored in a desiccator at 40 °C for 1 week under a relative humidity (RH) level of 75% by using a sodium chloride saturated salt solution to study the effect of humidity on the stability of these two compounds.

Proton Nuclear Magnetic Resonance (^{1}H NMR). Spectra were recorded on a Bruker AMX 300 Advance spectrometer. Samples were dissolved in deuterated dimethyl sulfoxide (DMSO-d_6) (^{1}H at 300 MHz). Chemical shifts are given in parts per million (ppm) relative to the given solvent. The multiplicity is as follows: s = single, d = doublet, dd = doublet of doublets, t = triplet, q = quartet. All of the data were acquired and processed with MestReNova.

Powder X-ray Diffraction (PXRD). PXRD data were collected using a Siemens D5000 powder X-ray diffractometer with Cu Kα radiation (λ = 1.54056 Å), with 35 kV and 45 mA voltage and current applied. An amount of powder was gently pressed on a glass slide to afford a flat surface and then analyzed. The samples were scanned from 2θ = 2−50° using a step size of 0.02° and a scan rate of 1°/s.

Single-Crystal X-ray Diffraction (SC-XRD). Suitable crystals of **1·URE**, **1·DHB**, and **4HB·H$_2$O** were selected for X-ray single-crystal diffraction experiments and mounted at the tip of a glass fiber on an Enraf-Nonius CAD4 diffractometer producing graphite-monochromated MoKα radiation (λ = 0.71073 Å). After a random search of 25 reflections, an indexation procedure gave rise to the cell parameters. Intensity data were collected in the ω−2θ scan mode and corrected for Lorenz and polarization effects at 294(2) K. The structural resolution procedure was made using the WinGX package.[36] The solution of structure factor phases was performed with SHELXS-2013,[37] except for **1·URE**, for which SIR2014[38] was used, and the full matrix refinement was carried out with SHELXL2014/7.[37] Non-H atoms were refined anisotropically. For **1·DHB**, the aliphatic chain of the uracil (ethyl

https://doi.org/10.1021/acs.cgd.1c00175
Cryst. Growth Des. 2021, 21, 4857−4870

Table 1. General and Crystallographic Data for Cocrystals 1·URE, 1·MAL, 1·TAR, 1·SAL, 1·4HB_FII, and 1·DHB and Coformer 4HB·H_2O

	1·URE	1·MAL	1·TAR	1·SAL	1·4HB_FII	1·DHB	4HB·H_2O
molecular formula	$C_7H_{12}N_4O_3$	$C_{16}H_{22}N_4O_9$	$C_{16}H_{22}N_4O_{10}$	$C_{13}H_{14}N_2O_5$	$C_{13}H_{14}N_2O_5$	$C_{13}H_{14}N_2O_6$	$C_6H_{10}N_2O_3$
formula mass	200.21	414.37	430.37	278.26	278.26	294.26	156.13
cryst syst	monoclinic	triclinic	triclinic	triclinic	triclinic	orthorhombic	triclinic
space group	$P2_1/c$	$P1$	$P1$	$P\bar{1}$	$P\bar{1}$	$Pnma$	$P\bar{1}$
a/Å	4.981(4)	7.010(5)	6.9897(10)	7.458(4)	7.6435(6)	14.3590(19)	6.186(4)
b/Å	13.264(5)	8.166(6)	8.2046(11)	8.072(5)	7.8752(6)	6.797(3)	6.898(6)
c/Å	14.555(6)	9.062(7)	9.0659(13)	11.598(7)	10.8760(8)	13.880(3)	8.910(4)
α/deg	90	82.511(15)	83.135(2)	71.510(9)	90.140(3)	90	102.02(10)
β/deg	93.61(5)	67.387(14)	68.120(2)	78.728(9)	104.635(2)	90	103.67(6)
γ/deg	90	79.049(15)	79.314(2)	84.409(9)	94.228(3)	90	94.77(6)
V/Å^3	959.7(9)	469.2(6)	473.37(12)	648.9(6)	631.56(8)	1354.7(7)	357.8(4)
T/K	294(2)	294(2)	294(2)	294(2)	100.0	294(2)	294(2)
Z	4	1	1	2	2	4	2
D_{calc}/g cm^{-3}	1.386	1.467	1.510	1.424	1.463	1.443	1.449
μ/mm^{-1}	0.110	0.121	0.127	0.111	0.964	0.116	0.120
F(000)	424	218	226	292	292.0	616	164
no. of collected/unique rflns	1745/1679	10230/4642	7308/4127	7763/2998	36973/2223	2591/1294	1468/1264
no. of data/restraints/params	1679/0/148	4642/3/284	4127/3/277	2298/0/185	2223/0/184	1294/0/144	1264/3/117
$\Delta\rho_{max}$, $\Delta\rho_{min}$/e Å^3	0.15, −0.142	0.155, −0.169	0.20, −0.21	0.20, −0.20	0.20, −0.21	0.175, −0.149	0.241, −0.195
R ($F^2 > 4\sigma(F^2)$)	0.0461	0.0491	0.0552	0.0397	0.0366	0.0403	0.0467
R_w (F^2)	0.1242	0.1177	0.1192	0.1122	0.0947	0.1188	0.1348
goodness of fit, S	1.036	1.028	1.096	1.065	1.102	1.019	1.071

substitution, C7 and C8) was split into two equivalent positions (50% fractional occupancy) to account for the observed disorder. For **1·DHB**, H atoms were introduced in calculated positions, except those of hydroxyl groups, which were found in a Fourier map and refined riding on their parent atoms. For **4HB·H_2O**, H atoms were introduced in calculated positions and refined riding on their parent atoms, except for those bound to oxygen atoms, which were located in the Fourier map and refined isotropically with $U_{iso}(H) = 1.5U_{eq}(O)$. For **1·URE**, H atoms were introduced in calculated positions and refined riding on their parent atoms, except for those bound to nitrogen atoms, which were located in the Fourier map and refined isotropically with $U_{iso}(H) = 1.5U_{eq}(N)$.

A suitable crystal of **1·MAL** was selected for an X-ray single-crystal diffraction experiment and mounted at the tip of a nylon CryoLoop on a BRUKER APEX-II CCD diffractometer using graphite-monochromated Mo Kα radiation (λ = 0.71073 Å). Crystallographic data were collected at 294(2) K. Frames taken with a 0.3° separation afforded 10230 reflections up to $2\theta_{max}$ value of ca. 56°. Data reduction was performed using SAINT V6.45A and SORTAV[39] in the diffractometer package. Data were corrected for Lorentz and polarization effects and for absorption by SADABS.[40] The structural resolution procedure was carried out using SHELXT.[41] Non-H atoms were refined anisotropically. H atoms were introduced in calculated positions, except those of hydroxyl groups, which were found in a Fourier map and refined riding on their parent atoms.

Suitable crystals of **1·TAR** and **1·SAL** were selected for X-ray single-crystal diffraction experiments, covered with oil (Infineum V8512, formerly known as Paratone N), and mounted at the tip of a nylon CryoLoop on a Bruker-Nonius X8 APEX-II KAPPA CCD diffractometer using graphite-monochromated Mo Kα radiation (λ = 0.7107 Å). Crystallographic data were collected at 294(2) K. Data were corrected for Lorentz and polarization effects and for absorption by SADABS.[40] A suitable crystal of **1·4HB _FII** was selected, covered with oil (Infineum V8512, formerly known as Paratone N), and mounted at the tip of a nylon CryoLoop on a Bruker D8 Venture diffractometer using Cu Kα radiation (λ = 1.54178 Å). The crystal was kept at 100 K during data collection. Using Olex2,[42] the structure was solved with the XT structure solution program using intrinsic phasing and refined with the XL refinement package using least-squares minimization.[37] Non-H atoms were refined anisotropically. H atoms were introduced in calculated positions and refined riding on their parent atoms.

The structures were checked for higher symmetry with the help of the program PLATON.[43] In Table 1 general and crystallographic data for the new cocrystals and 4-hydroxybenzoic acid monohydrate are summarized. Hydrogen-bond parameters for all of the solved structures can be found in Table S1 in the Supporting Information.

Thermogravimetric Analysis–Differential Scanning Calorimetry (TGA-DSC). Thermal analyses were carried out on a simultaneous thermogravimetric analysis (TGA)–differential scanning calorimetry/differential thermal analysis (heat flow DSC/DTA) NETZSCH -STA 449 F1 Jupiter system. Samples (3–8 mg) were placed in an alumina pan and measured at a scan speed of 10 °C min^{-1} from ambient temperature to 250 °C under an N_2 atmosphere as a protective and purge gas (their respective flow velocities were 20 and 40 mL/min).

Attenuated Total Reflection Fourier Transform Infrared Spectroscopy (ATR-FT-IR). Infrared spectra were recorded with a Jasco 4700LE spectrophotometer with an attenuated total reflectance accessory. The scanning range was 4000 to 400 cm^{-1} at a resolution of 4.0 cm^{-1}.

Theoretical Calculations. The theoretical study reported herein was carried out using the Gaussian-16[44] program package and the PBE1PBE-D3/def2-TZVP level of theory.[45] Since we intend to estimate the interactions in the solid state, the crystallographic coordinates have been used. This level of theory and methodology have previously been used to evaluate similar interactions.[46−48] In this work the binding energy and interaction energy terms have been used interchangeably. They were computed as the difference between the energies of the isolated monomers and their assembly and were corrected for the basis set superposition error (BSSE) by using the Boys–Bernardi counterpoise method.[49] Bader's quantum theory of "atoms in molecules" (QTAIM) and the noncovalent interaction index (NCIPlot) have been used to characterize the noncovalent interactions using the AIMall program.[50] The molecular electrostatic potential (MEP) surfaces have been generated using the Gaussian-16 software and the PBE1PBE-D3/def2-TZVP wave functions. The 0.001 au isosurface has been used as the best estimate of the van der Waals surface.

https://doi.org/10.1021/acs.cgd.1c00175
Cryst. Growth Des. 2021, 21, 4857−4870

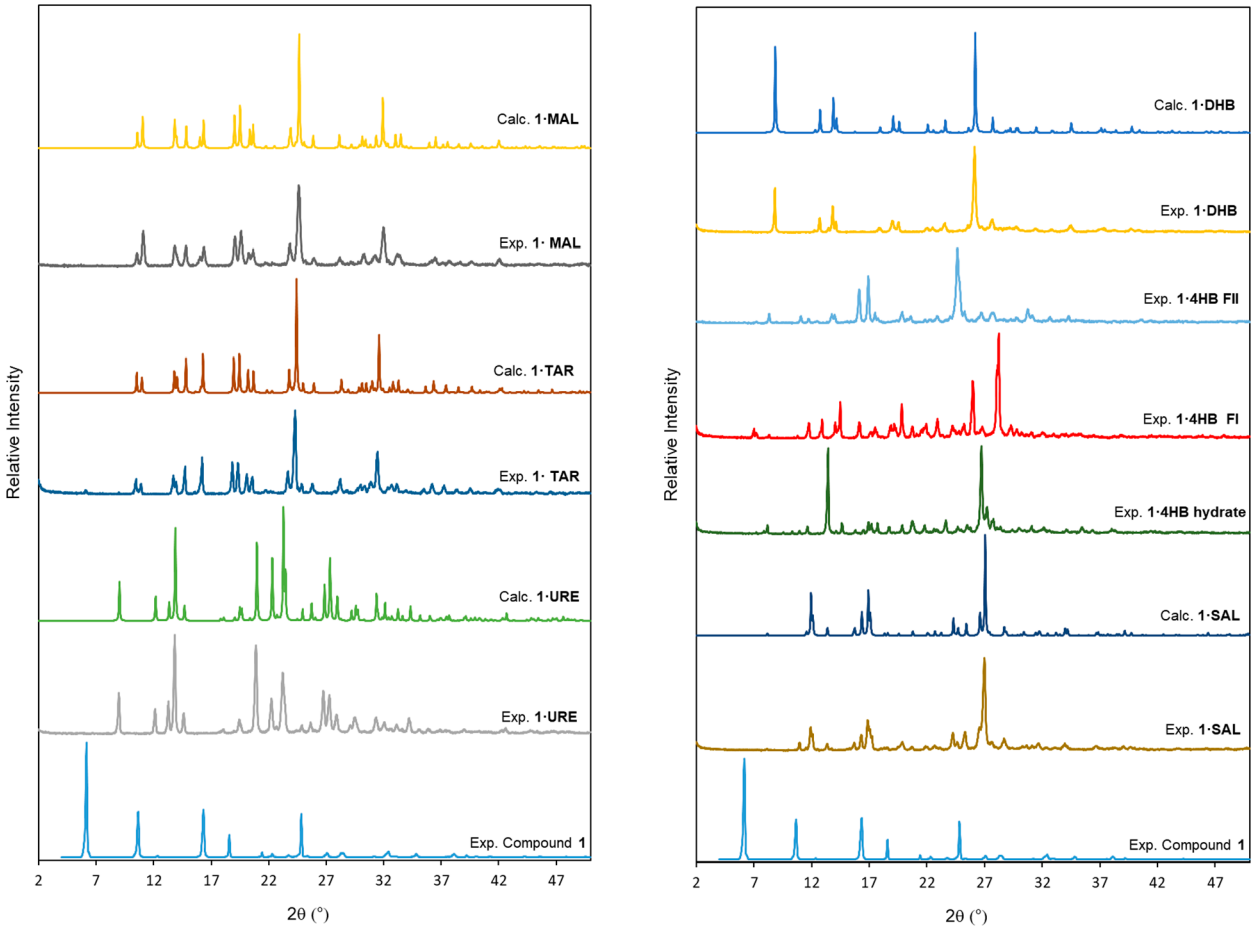

Figure 1. Comparison of the experimental and calculated PXRD patterns of **1** and the as-synthesized cocrystals **1·URE**, **1·TAR**, **1·MAL**, **1·SAL**, **1·4HB·H_2O**, **1·4HB_FI**, **1·4HB_FII**, and **1·DHB**.

RESULTS AND DISCUSSION

Powder X-ray Diffraction. Figure 1 presents the experimental and the calculated PXRD patterns for 1-ethyluracil and the prepared cocrystals showing the excellent agreement among them. Moreover, they also indicate the purity of the resulting solids by the absence of the respective former compounds after grinding.

It is interesting to note that the powder patterns of the as-synthesized cocrystals **1·MAL** and **1·TAR** show many characteristic features in common, rendering what is known as isostructural solids.[51] The formation of isostructural cocrystals or salts due to the presence of solvent molecules or because of the similarity among coformers is not an uncommon process, and several interesting examples have been well described in the literature.[52,53] The resemblance between L-malic and L-tartaric acids is considerable, and this isostructurality according to their powder diffractograms means that the presence of an additional hydroxyl group in the L-tartaric acid with respect to L-malic acid does not greatly alter its tridimensional network but reinforces it. The *crystal structural similarity* (CSS) tool from Mercury (Materials module) of the CSD applied to two cocrystal structures resulted in the structures being isostructural within the distance and angle default tolerance values of 20% and 20°, respectively, and with a default size of the molecular cluster of 15 molecules (the central molecule plus 14 others). With this set of parameters, a root-mean-square deviation (RMSD) of 0.057 and a PXRD similarity index of 0.992 were obtained, which is very close to 1, the highest value for identical patterns. Furthermore, the *unit-cell similarity index* (Π) was also calculated by a previously described method.[54,55] When Π is close to zero, the two unit cells are very similar. In our case, a Π value of as low as 0.001 was obtained. Thus, both compounds are both isostructural and isomorphous.

The use of 4-hydroxybenzoic acid has allowed us to identify three different forms (Figure 1). LAG in the presence of water afforded a crystalline solid (**1·4HB·H_2O**), which was concluded to be a hydrated form according to its TGA trace (Figure S1). However, the use of methanol during the grinding process gave a different XRD pattern (**1·4HB_FII**). On this occasion it was an anhydrous form, as no weight loss was observed before degradation during its thermogravimetric analysis (see Figure S1). Moreover, drying **1·4HB·H_2O** at 50 °C under vacuum gave a new solid (**1·4HB_FI**), different from its parent compounds or **1·4HB_FII**, which was also anhydrous. This means that a second anhydrous crystalline form between 1-ethyluracil and 4-hydroxybenzoic acid molecules was obtained (Figure S1). Numerous efforts were made in order to obtain single crystals of the three forms to confirm these observations. Nevertheless, only adequate single crystals of **1·4HB_FII** were obtained. In contrast, single crystals of the coformer 4-hydroxybenzoic acid monohydrate were obtained and will be discussed in the next section. The stability of these two anhydrous forms was explored under 75% relative humidity at 40 °C for 1 week. The PXRD analyses for the two solids after this period showed that both

https://doi.org/10.1021/acs.cgd.1c00175
Cryst. Growth Des. 2021, 21, 4857−4870

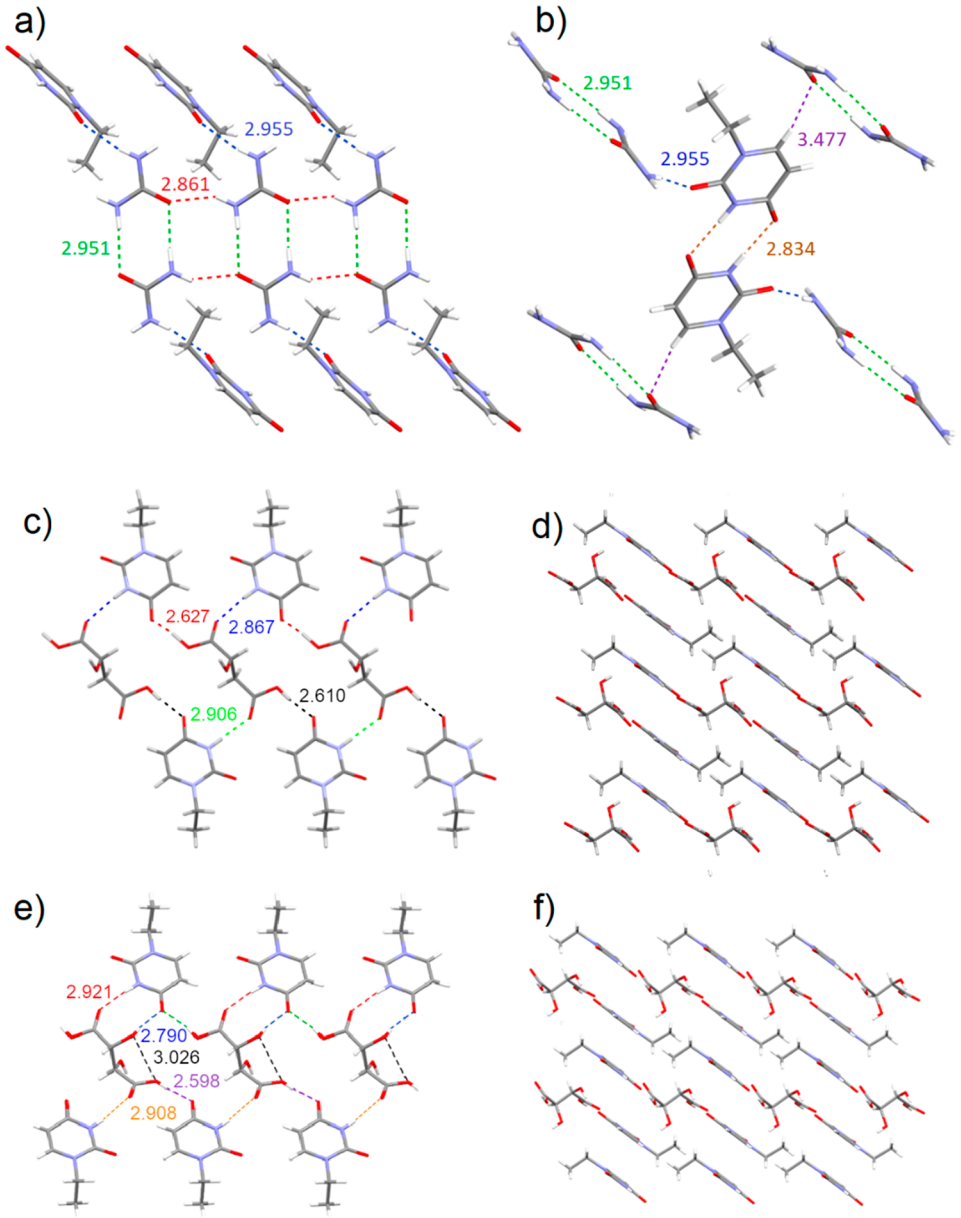

Figure 2. (a) Urea double chains along the *a* axis with their respective stacked 1-ethyluracils. (b) Self-assembly of a 1-ethyluracil and aromatic CH interaction with urea. (c) Interactions among 1-ethyluracil and L-malic acid molecules and (d) $\pi-\pi$ stacking. Interactions between L-tartaric acid and 1-ethyluracil, forming (e) chains and (f) $\pi-\pi$ stacking. Distances shown are in Å.

forms were stable, as they did not transform into the hydrated cocrystal.

Crystal Structure Descriptions. ***1·URE.*** The cocrystal was prepared by slow evaporation from a nitromethane−ethanol solution at room temperature. The crystal structure of this compound was solved and refined in the monoclinic space group $P2_1/c$ containing one molecule of 1-ethyluracil and a molecule of urea in the asymmetric unit. In the supramolecular structure, hydrogen bonds were formed by homosynthons between two 1-ethyluracil molecules (imide−imide) or urea−urea molecules (amide−amide) and heterosynthons (amide−imide) in urea−1-ethyluracil. The overall structure consists of columns of face-to-face urea molecules and columns of 1-ethyluracil molecules as shown in Figure 2.

The interactions with successive urea molecules form an infinite double chain through the *a* axis (see Figure 2a) with hydrogen bonds along the chain direction (N(4)−H···O(1) distance, 2.861(3) Å (in red); angle, 150(2)°) and along the sides to form the double chain (N(4)−H···O(1) distance, 2.951 Å (in green); angle, 176(2)°). The remaining nitrogen atom is bound to 1-ethyluracil through N(2)−H···O(2) (distance, 2.955(4) Å (in blue); angle, 171(3)°). This chain is further reinforced through $\pi-\pi$ stacking within 1-ethyluracil molecules ($\pi-\pi$ interplanar distance 3.377 Å). Chains are communicated by uracil molecules in a self-assembling arrangement, forming planes parallel to the *ac* plane (N(3)−H···O(4) distance, 2.834(3) Å (in orange in Figure 2b); angle, 177(2)°). Planes are connected through the hydrogen bond established between uracil and the aromatic CH in the sixth position of 1-ethyluracil (C(6)−H···O(1) distance, 3.477(3) Å (in purple); angle, 158.5°) (see Figure 2b).

1·MAL. Single crystals were afforded in nitromethane after slowly heating the mixture and cooling it to room temperature. The cocrystal crystallizes in the triclinic space group *P*1

https://doi.org/10.1021/acs.cgd.1c00175
Cryst. Growth Des. 2021, 21, 4857−4870

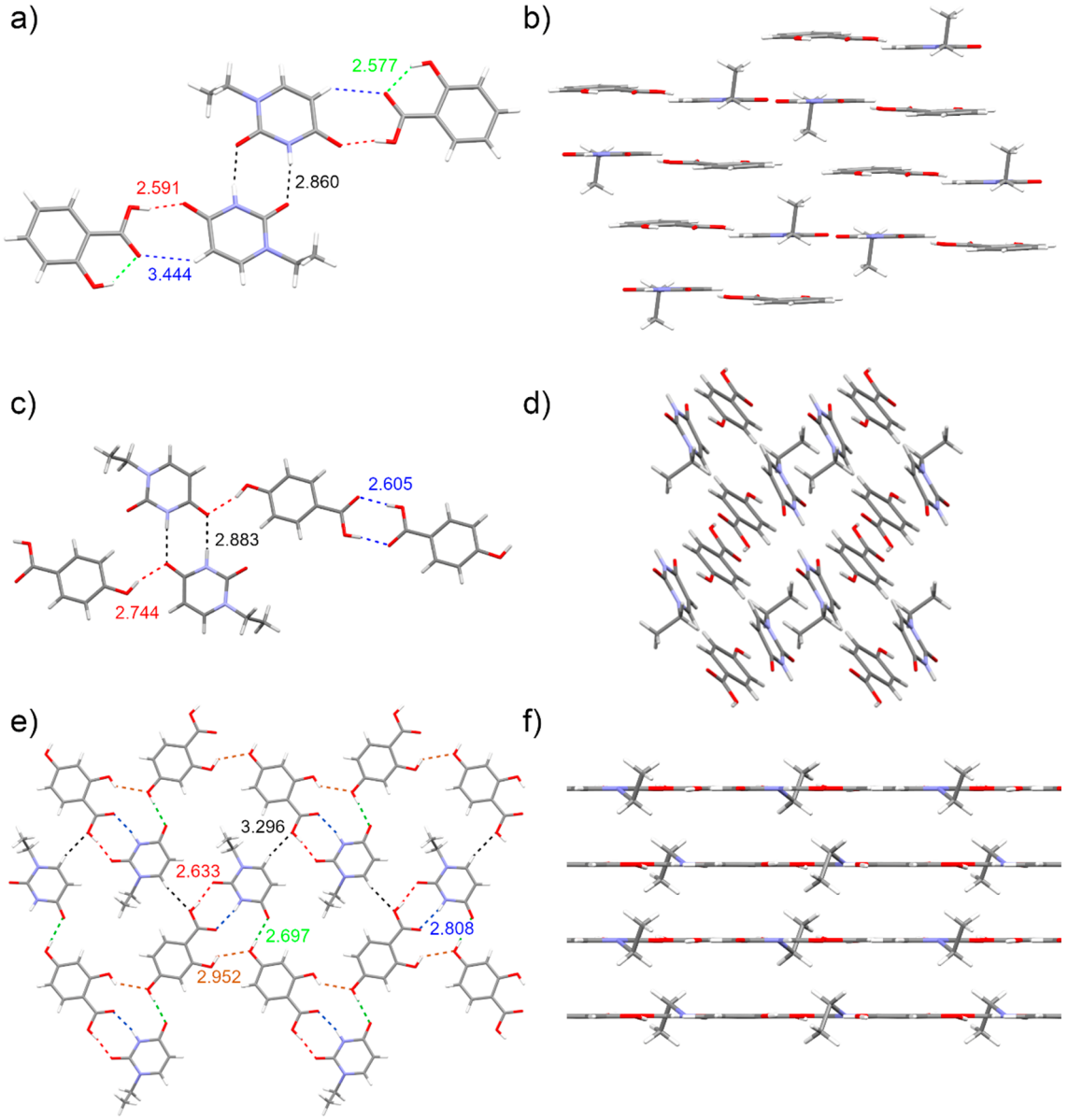

Figure 3. Chains (a) and stacking (b) observed in **1·SAL**. (c) Contacts and d) packing in **1·4HB FII**. Planes (e) and stacking (f) formed in the cocrystal **1·DHB** among 1-ethyluracil and DHB molecules. Only one orientation of the ethyl substituent in **1·DHB** is shown. Distances are shown in Å.

containing two molecules of 1-ethyluracil and a molecule of L-malic acid in the asymmetric unit. No solvent molecules are observed, confirming the anhydrous state determined by thermal methods.

L-Malic acid acts as a bridge between two 1-ethyluracil molecules. From one side, hydrogen bonds among the −OH group from carboxylic acid and O═C from 1-ethyluracil were established through O(6)−H···O(14)═C (distance, 2.610(5) Å (in black); angle, 172.8°) and O(1)−H···O(14)═C (distance, 2.627(5) Å (in red); angle, 173(4)°) interactions. There were also hydrogen bonds through the carbonyl from the carboxylic acid by C═O(3)···H−N(3) (distance, 2.867(6) Å (in blue); angle, 179.2°) and C═O(7)···H−N(13) (distance, 2.906(6) Å (in green); angle, 167.0°) contacts.

Moreover, in this structure the −OH group from malic acid is disordered and presents two possible orientations with 75% and 25% occupation factors. Both disordered positions are *S* chiral centers, as expected for the reactant L-malic acid. This also confirms the noncentrosymmetric space group *P*1. This substituent established further hydrogen bonds with a carbonyl from the modified nucleobase through O(5)(H···O(2)═C (distance, 2.806(5) Å; angle, 175.1°) and O(5A)−H···O(4)═C (distance, 2.989(14) Å; angle, 168.8°).

No hydrogen bonds are observed among 1-ethyluracil molecules. However, a $\pi-\pi$ interaction is established: the electronegative carbonyl groups interact with the electropositive central region of the aromatic orbital deployed both above and below the ring (O(2)···centroid, 3.351 Å; O(12)···centroid, 3.340 Å; O(14)···centroid, 3.451 Å; O(4)···centroid, 3.438 Å), as shown in Figure 2d. Further contacts are formed, as shown in Table S1.

1·TAR. This crystal was prepared by antisolvent crystallization from an ethanol−cyclohexane mixture. The crystal structure of this compound was solved and refined in the triclinic space group *P*1, containing two molecules of 1-ethyluracil and a molecule of L-tartaric acid in the asymmetric unit. No solvent

https://doi.org/10.1021/acs.cgd.1c00175
Cryst. Growth Des. 2021, 21, 4857−4870

molecules are observed. As noted previously in the Powder X-ray Diffraction section, **1·TAR** and **1·MAL** are isostructural, which is confirmed by an analysis of the hydrogen-bonding interactions obtained by SC-XRD in each cocrystal. In a fashion similar to that of the cocrystal with L-malic acid, herein the dicarboxylic coformer L-tartaric acid also acts as a bridge between two 1-ethyluracil units, establishing hydrogen bonds first among O−H groups from carboxylic acids and C(4)═O groups in 1-ethyluracil, H21 and O4 (O(21)−H···O(4) distance, 2.599(4) Å (in purple); angle, 165.3°) and H26 and O14 (O(26)−H···O(14) distance, 2.621(5) Å; angle, 164.5°) (see Figure 2e), and second among the carbonyl groups from carboxylic units and the free N−H units from 1-ethyluracil, N(13)−H···O(25) (distance, 2.921(5) Å (in red); angle, 175.3°) and N(3)−H···O(22) (distance, 2.908(5) Å (in orange); angle, 165.4°).

L-Tartaric acid establishes further interactions through its two alcohol substituents to the C(4)═O group from 1-ethyluracil molecules: O(24)−H···O(14)−C (distance, 2.790(5) Å (in blue); angle, 158.0°) and O(23)−H···O(12)-C (distance, 2.845(4) Å; angle, 169.8°).

Similarly to **1·MAL**, the cocrystal does not form hydrogen bonds between 1-ethyluracil molecules. However, again a certain $\pi-\pi$ interaction is established; the electronegative carbonyl groups interact with the electropositive central region of the aromatic orbital deployed both above and below the ring (for instance: O(12)···centroid, 3.351 Å; O(2)···centroid, 3.328 Å or O(14)···centroid, 3.602 Å; O(4)···centroid, 3.516 Å), as shown in Figure 2f. Further contacts are observed, as shown in Table S1.

1·SAL. This cocrystal was prepared by slow evaporation from a methanol−water solution (1:1). The new compound crystallized in the triclinic system with space group $P\bar{1}$. The asymmetric unit consists of a 1-ethyluracil molecule and a salicylic acid molecule.

In this case, 1-ethyluracil molecules present a self-assembling arrangement using its Watson−Crick edge by tandem N(3)−H···O(2) hydrogen bonds (distance, 2.8600(17) Å (in black); angle, 168.8°). The interaction between 1-ethyluracil and salicylic acid is established through the Hoogsteen edge with the acid group edge (O(18)−H···O(4) distance, 2.5911(16) Å (in red); angle, 165.1°; C(5)−H···O(17) distance, 3.444(2) Å (in blue); angle, 144.0°). Salicylic acid also establishes an intramolecular hydrogen bond within its hydroxyl group and its acid group (O(12)−H···O(17) distance, 2.5770(19) Å (in green); angle, 146.2°). These interactions can be seen in Figure 3a.

The planes formed through the described interactions are then piled on top of each other, thanks to stacking interactions between 1-ethyluracil and salicylic acid molecules (N(3)··· salicylic acid centroid distance, 3.322 Å), thus completing the whole structure as seen in Figure 3b.

1·4HB_FII. A suitable single crystal was obtained from slow evaporation of a mixture of acetonitrile and *n*-propyl acetate. The compound crystallized in the triclinic space group $P\bar{1}$. A molecule of 1-ethyluracil and a molecule of 4-hydroxybenzoic acid are included in the asymmetric unit.

In this case, two different homosynthons were observed in the supramolecular structure: those formed by self-assembly between 1-ethyluracil molecules (C(4)═O(4)···H−N(3) distance, 2.8831(15) Å (in black); angle, 172.9°) and between 4-hydroxybenzoic acid coformers by a strong carboxylic acid−carboxylic acid synthon (O(18)−H(18)···O(17) distance, 2.6051(14) Å (in blue); angle, 173.4°) (Figure 3c). Moreover, the nucleobase and the coformer interact through the carbonyl from 1-ethyluracil and the hydroxyl group from the 4HB molecule (C(4)═O(4)···H(14)−O(14): distance, 2.7434(14) Å (in red); angle, 160.1°). These zigzag tapes are interconnected, forming planes by further interactions through the second carbonyl from 1ETURA and the aromatic C(13)−H from 4HB (C(2)═O(2)····H−C(13): distance, 3.294 Å; angle, 149.44°) or C(6)−H from the nucleobase and the carbonyl from carboxylic acid in the coformer 4HB (C(17)═O(17)···· H−C(6): distance, 3.330 Å; angle, 142.54°). Finally, the tridimensional structure is accomplished by piling of these sheets through $\pi-\pi$ stacking among the uracil and aromatic rings from the coformer.

1·DHB. A cocrystal (1:1) of 1-ethyluracil and 2,4-dihydroxybenzoic acid was identified from solvent evaporation performed in a water−methanol (1:1) solution. This compound crystallized in the orthorhombic space group *Pnma*. The asymmetric unit consists of one molecule of 1-ethyuracil and one molecule of 2,4-dihydroxybenzoic acid.

In this structure, 1-ethyluracil interacts mainly with 2,4-dihydroxybenzoic acid, forming chains parallel to the *c* axis (see Figure 3c). The acid group of 2,4-dihydroxybenzoic acid forms two hydrogen bonds with O(2) and N(3) of 1-ethyluracil (O(1)−H···O(2) distance, 2.633(3) Å (in red); angle 175(4)°; N(3)−H···O(3) distance, 2.808(3) Å (in blue); angle 168.8°). At the same time, an hydroxyl group in a *para* position from another 2,4-dihydroxybenzoic acid bonds to the hydroxyl group in an *ortho* position from the former 2,4-dihydroxybenzoic acid (O(5)−H···O(6) distance, 2.952(3) Å (in orange color); angle, 123(3)°) and to O(4) from 1-ethyluracil (O(6)−H···O(4) distance, 2.697(3) Å (in green); angle, 178(3)°). These chains are interconnected, forming planes parallel to the *bc* plane by another hydrogen bond, within the aromatic C(6) in 1-ethyluracil and the acid group in 2,4-dihydroxybenzoic acid (C(6)−H···O(1) distance, 3.296(3) Å (in black); angle, 167.5°).

The aliphatic substituent presents orientational disorder on both sides of the molecular plane as imposed by the space group mirror plane. The planes stack on top of one another through $\pi-\pi$ stacking within 1-ethyluracil and 2,4-dihydroxybenzoic acid molecules ($\pi-\pi$ interplanar distance, 3.397 Å). Chains can either be facing each other between planes, establishing van der Waals forces, or opposing. These two configurations alternate through the different planes (Figure 3d).

4HB·H$_2$O. During solvent evaporative crystallizations between 1-ethyluracil and 4-hydroxybenzoic acid, single crystals of the latter were obtained in a water−ethanol mixture as the solvent. The crystal structure obtained was triclinic with space group $P\bar{1}$ containing one molecule of 4-hydroxybenzoic acid and one molecule of water in the asymmetric unit. After a search in the Cambridge Structural Database (version 5.41, August 2020 update), our structure was found to be different from those described previously with refcodes PHBZAC04[56] and PHBZAC05[57] or that previously described by Fukuyama et al.[58] In our case, the supramolecular structure is obtained by carboxylic dimers in addition to water molecules participating in OH···OH bridges with the hydroxyl groups from 4-hydroxybenzoic acid and also with the carboxylic homosynthons, giving birth to planes (Figure S1a). The planes are further piled up by $\pi-\pi$ interactions ($\pi-\pi$ inteplanar distance, 3.437 Å), creating the full 3D molecular arrangement (Figure S1b).

https://doi.org/10.1021/acs.cgd.1c00175
Cryst. Growth Des. 2021, 21, 4857−4870

Spectroscopic Analysis of Cocrystals. 1-Ethyluracil, coformers, and the new compounds were analyzed by Fourier transform infrared spectroscopy in attenuated mode (ATR-FT-IR) to detect changes in the vibrational modes of the functional groups that could indicate new hydrogen-bonding interactions among parent compounds and thus indicate cocrystal formation. Their FTIR spectra are displayed in Figures S2−S7 in the Supporting Information.

The FTIR spectrum of compound **1** shows characteristic bands in the range between 3150 and 3000 (3147, 3090, and 3011) cm^{-1} for N−H, between 2980 and 2800 cm^{-1} for =CH, at 1772, 1739, and 1708 cm^{-1} for C=O, and at 1643 cm^{-1} for C=C. In the FTIR spectrum of urea, characteristic bands at 3427, 3328, and 3254 cm^{-1} (N−H) and 1674 cm^{-1} (C=O) are observed. After **1·URE** cocrystal formation, the FTIR spectrum (Figure S2) shows some increasing values for bands of N−H vibrations (at 3451, 3350, and 3191 cm^{-1}). Other changes are also observed for C=O and C=N stretching vibrations. These new bands confirm the participation of all these functional groups in the hydrogen bonds as deduced by the single-crystal resolution.

In the FTIR spectrum of L-tartaric acid, characteristic bands at 3400, 3329, and 3104 cm^{-1} for O−H (CHOH) and O−H (COOH) and at 1714 cm^{-1} for C=O are observed. However, the spectrum after grinding with compound **1** shows only a band at 3412 cm^{-1} for N−H and O−H vibrations and two overlapped broad, intense bands with maxima at 1683 and 1648 cm^{-1} for C=O and C=C stretching modes, respectively, confirming the new phase **1·TAR** (Figure S3).

The FTIR spectrum of L-malic acid shows typical vibrational bands at 3524, 3380, and 2957 cm^{-1} for hydroxyl groups from the chain and the carboxylic groups and at 2874 and 2671 cm^{-1} for −C−H (Figure S4). C=O stretching appears at 1686 cm^{-1} as a strong band. After cogrinding of **1** and L-malic acid, the IR spectrum of **1·MAL** shows only one band at 3393 cm^{-1} associated with the hydroxyl group. In the region of C=O, C=N and C=C vibrations, three strong bands at 1683, 1664, and 1640 cm^{-1} can be identified.

The FTIR spectrum of salicylic acid shows characteristic bands at 3231 and 3004 cm^{-1} for O−H from the phenol and at 2849 and 2532 cm^{-1} for O−H from carboxylic acid and C_{ar}−H. The C=O vibrational bands from the carboxylic group appear at 1654 and 1609 cm^{-1} and that of the C=C stretch at 1578 cm^{-1}. In the spectrum of the cocrystal **1·SAL**, the band at 3231 cm^{-1} from the salicylic acid has completely disappeared and even the C=O vibrational bands from the 1-ethyluracil and only a band at 1652 cm^{-1} is observed (see Figure S5), indicating that a new compound was obtained.

The next group of compounds consisted of the use of the coformer 4-hydroxybenzoic acid (Figure S6). In its FTIR spectrum, typical bands for vibrational modes at 3354 and 3054 cm^{-1} for O−H from the phenol and at 2947, 2811, 2653, and 2541 cm^{-1} for O−H (COOH) are observed. The C=O and C=C stretching bands appear at 1669, 1605, and 1592 cm^{-1}. In LAG experiments, the use of water or methanol afforded two different crystalline solids. When water was used , a hydrated cocrystal, **1·4HB·H_2O**, resulted, as confirmed by the presence of a band at 3498 cm^{-1} that can be assigned to the OH group from water molecules and another band at 3350 cm^{-1} for OH from 4-hydroxybenzoic acid. However, for the new **1·4HB_I** and **_II** no bands were observed in the OH region. This confirmed the formation of new interactions for these compounds with respect to the former compounds or even the hydrated cocrystal. In the range of 1800−1500 cm^{-1}, other changes can also be detected. The bands corresponding to C=O (at ca. 1772−1708 cm^{-1}) from 1-ethyluracil disappeared for the cocrystal **1·4HB·H_2O**, and only bands at 1664 and 1643 cm^{-1} appeared. Nevertheless, for the anhydrous forms some bands at 1700−1726 cm^{-1} can be observed in addition to peaks at 1670−1650 cm^{-1}.

Finally, in the FTIR spectrum of our last coformer, 2,4-dihydroxybenzoic acid, bands at 3358, 2955, 2847, and 2547 cm^{-1} are assigned to O−H and C−H stretching vibrations. The C=O and C=C vibrational modes appear at 1627 and 1520 cm^{-1}, respectively.[59] In the FTIR spectrum of the new compound **1·DHB**, the O−H band from the coformer and the C=O stretching mode from 1-ethyluracil have completely disappeared and only a band at 1664 cm^{-1} can be observed, thus confirming the formation of a new hydrogen-bonded compound (see Figure S7).

Thermal Analysis. Finally, to gain more insight into the physical properties, all of the new forms prepared and 1-ethyluracil were analyzed with a simultaneous thermogravimetric analysis (TGA)−differential scanning calorimetry/differential thermal analysis (DSC/DTA). The TGA-DSC thermograms are shown in Figures S8−S14 in the Supporting Information. Relevant data such as temperatures of melting (as T_{peak}) for the new cocrystals and former compounds (1-ethyluracil and coformers) are summarized in Table 2.

Table 2. Melting Points of Compound 1, Coformers, and the New Cocrystals

compound	mp (°C)	coformer	mp (°C)[b]
1	144.9		
1·URE	130.6	URE	133
1·MAL	104.9	MAL	130
1·TAR	120.2	TAR	171−174
1·SAL	104.2	SAL	158.6
1·4HB-H_2O	72.3, 125.6[a]	4HB	214.5
1·4HB_FI	126.9		
1·4HB_FII	116.5		
1·DHB	173.8	DHB	208−211

[a]Desolvation and melting. [b]Sigma-Aldrich.

The TGA traces for **1** and all the other cocrystals have little loss on dryings (lod) before degradation takes place, except for the cocrystal **1·4HB-H_2O**, which confirms the unsolvated state of 1-ethyluracil and these new cocrystals. For **1·4HB-H_2O**, a 2% loss on drying (calculated 2.1% for 1/3·H_2O) was observed, corresponding to a dehydration process, which was accompanied by an endothermic peak at a T_{peak} value of 72.3 °C in the DSC thermogram, followed by a melting process (T_{peak} = 125.6 °C). This observation agrees with the thermal behavior observed for **1·4HB_FI**. For all of the other cocrystals only a single endotherm was observed in their respective DSC traces, attributed to the melting of the multicomponent solids followed by degradation.

Frequently, melting points are used as an indicator of the relative stability of the new compounds versus the parent formers. According to the results obtained herein, all of the new multicomponent solids showed melting peaks lower than those of the former 1-ethyluracil and their respective coformers, except for the **1·DHB** cocrystal. The melting temperature of **1·DHB** lies between the melting peaks of its precursors. Thus, the cocrystal **1·DHB** shows a better thermal stability in comparison to the modified nucleobase selected for this study.

https://doi.org/10.1021/acs.cgd.1c00175
Cryst. Growth Des. 2021, 21, 4857−4870

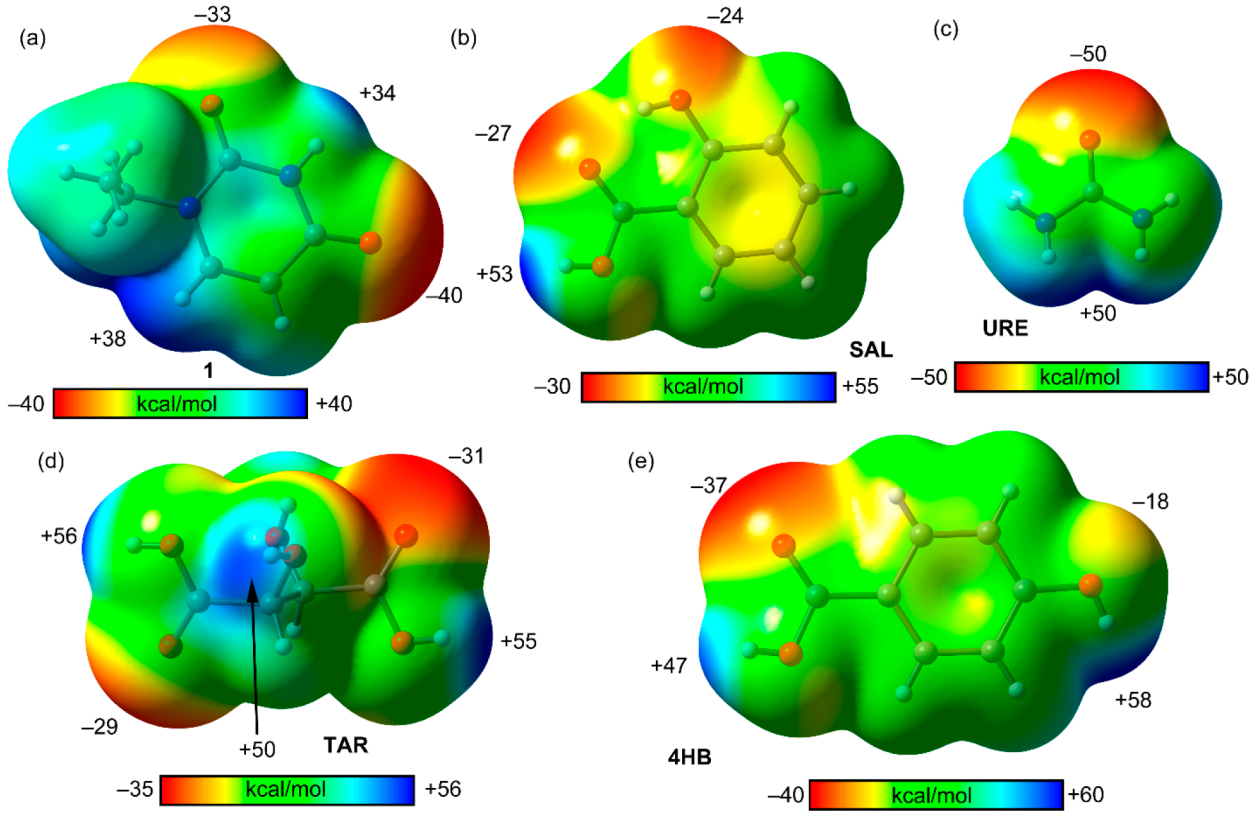

Figure 4. MEP surfaces of **1** (a), **SAL** (b) **URE** (c), **TAR** (d), and **4HB** (e) at the PBE1PBE-D3/def2-TZVP level of theory. Isosurface: 0.001 au. The values at selected points of the surface are given in kcal/mol.

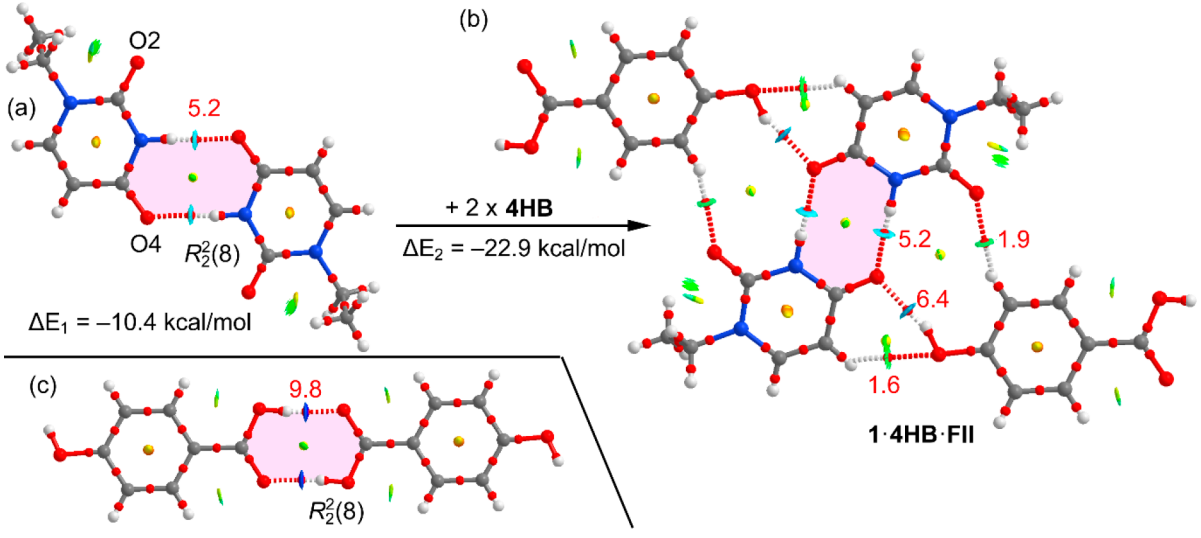

Figure 5. (a) QTAIM distribution of bond and ring CPs (red and yellow spheres, respectively) and NCIplot of the $R_2^2(8)$ dimer of **1·4HB_FII**. (b) QTAIM distribution of bond and ring CPs (red and yellow spheres, respectively) and NCIplot of the tetramer of **1·4HB**. (c) $R_2^2(8)$ dimer of the **4HB** coformer in compound **1·4HB_FII**. The dissociation energies of the H-bonds derived from the G_r values are indicated in red (in kcal/mol). The formation energies (ΔE) computed at the PBE1PBE-D3/def2-TZVP level of theory are also indicated.

DFT Calculations. In this theoretical study we analyze the energetic features of several supramolecular assemblies observed in the solid state of the cocrystals, focusing on some recurrent motifs and assigning individual energies to the different H-bonding interactions. This analysis is convenient to evaluate the relative importance of the interactions that govern the crystal packing and to give insight into the ability of uracil to participate in H-bonding networks with itself (self-assembly) and/or hydrogen bond donor groups.

Figure 4 shows the molecular electrostatic potential of compound **1** and several of the coformers used in this work. It can be observed that in compound **1** the most negative atom is the O4 atom (−40 kcal/mol) followed by the O2 atom (−33 kcal/mol) and the most positive value corresponds to the C−H group adjacent to N1 (+38 kcal/mol) followed by the N−H

https://doi.org/10.1021/acs.cgd.1c00175
Cryst. Growth Des. 2021, 21, 4857−4870

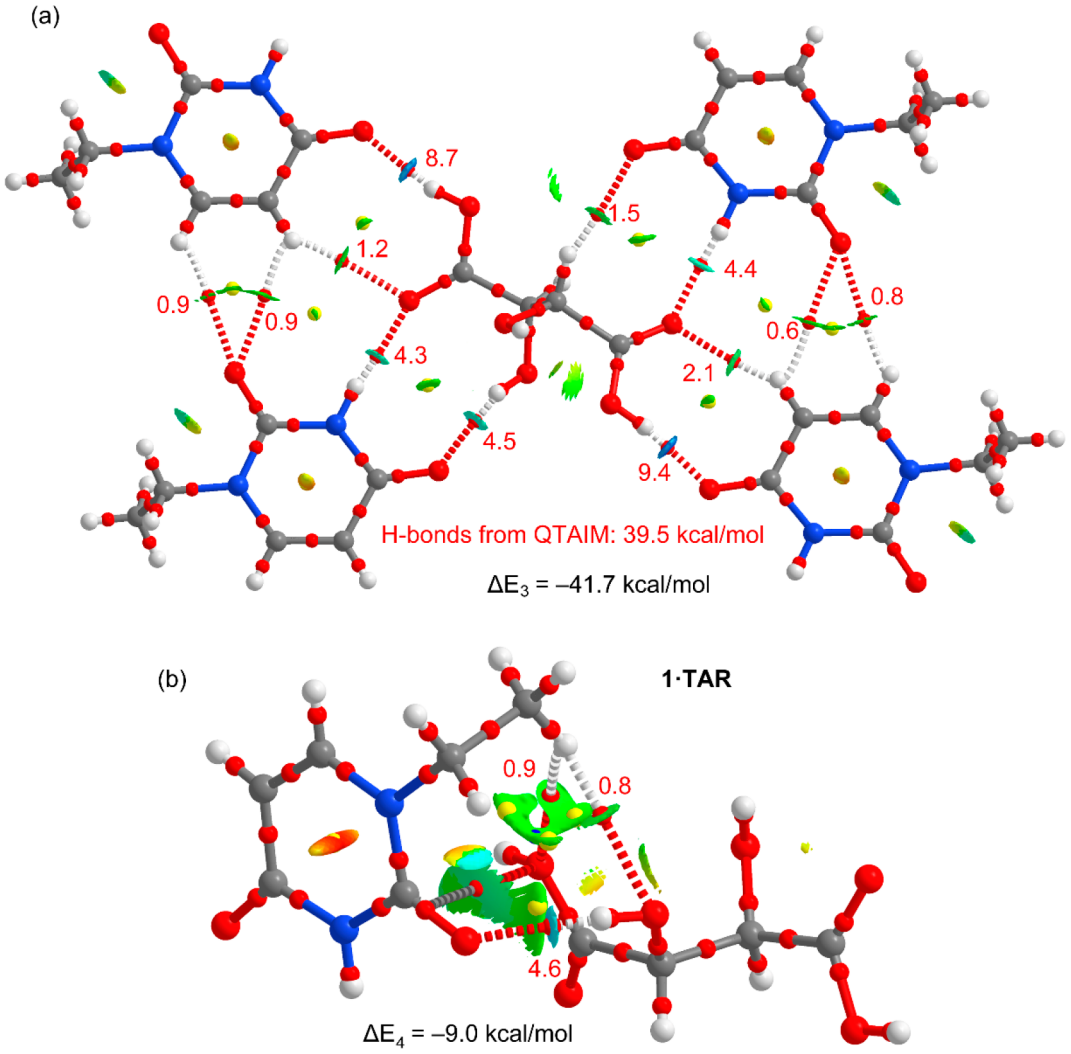

Figure 6. (a) QTAIM distribution of bond and ring CPs (red and yellow spheres, respectively) and NCIplot of the pentamer retrieved from the X-ray structure of **1·TAR**. (b) QTAIM distribution of bond, ring, and cage CPs (red, yellow, and blue spheres, respectively) and NCIplot of a dimer of **1·TAR**. The dissociation energies of the H-bonds derived from the G_r values are indicated in red (in kcal/mol). The formation energies (ΔE) computed at the PBE1PBE-D3/def2-TZVP level of theory are also indicated.

group, which has a value that is slightly lower (+34 kcal/mol). The MEP is more positive at the C−H group due to the influence of the adjacent CH_2 group of the ethyl group (the MEP merges at the same spatial region). With regard to the coformers, urea is the molecule of the series that presents identical (in absolute value) maximum and minimum MEP values (±50 kcal/mol): at the O atom, the minimum, and in the middle of both NH_2, groups the maximum. The most positive MEP values in this series are located on the acidic H atoms of the carboxylic groups (+47 to +56 kcal/mol) and the phenolic H atom of **4HB** (+58 kcal/mol). The MEP values at the O atoms of the carboxylic groups (ranging from −27 to −37 kcal/mol) and phenolic groups (−18 and −24 kcal/mol) are smaller than those of the O atoms of **1** (−33 and −40 kcal/mol) and urea (−50 kcal/mol). This MEP analysis anticipates that the H-bonding networks observed in the solid state of the cocrystals and compound **1** are expected to be energetically very strong.

Figure 5a shows the uracil $R_2^2(8)$ dimer observed in the solid state of **1·4HB_FII**. The interaction energy of the dimer ΔE_1 = −10.4 kcal/mol (using the X-ray geometry of **1·4HB FII**), thus indicating that each H-bond is moderately strong. Interestingly this $R_2^2(8)$ dimer establishes two symmetrically equivalent and strong O−H···O H-bonds with two adjacent 4-hydroxybenzoic acid molecules and two additional C−H···O bonds involving the aromatic C−H bonds. The formation energy of the tetramer from the $R_2^2(8)$ motif dimer is ΔE_2 = −22.9 kcal/mol. The assembly has been characterized using the quantum theory of atoms in molecules (QTAIM) in combination with the NCIplot index. The QTAIM shows that each H-bond is characterized by a bond CP that connects the O atom to the H atom belonging to an O−H, N−H, or C−H group. The individual energetic contribution of each hydrogen bond (dissociation energy) was also calculated using the kinetic energy density (G_r) value measured at the bond (CP) that characterizes the H-bond. It has been estimated according to the approach by Vener et al.[60] that was explicitly developed for H-bonds (energy = 0.429G_r). For pure closed-shell H-bonds, this proportionality is equivalent to that with the parallel curvature of the electron density $\lambda_3(r_{CP})$, as $G(r_{CP})$ is linearly related with $\lambda_3(r_{CP})$.[61,62] The individual dissociation energy of each H-bond is given in red in Figure 5. For the tetramer, the strongest H-bonds correspond to O−H···O (6.4 kcal/mol) followed by N−H···O (5.2 kcal/mol) of the $R_2^2(8)$ motif. This is also confirmed by the NCIplot method, which shows blue isosurfaces located between the O and H−O/

https://doi.org/10.1021/acs.cgd.1c00175
Cryst. Growth Des. 2021, 21, 4857−4870

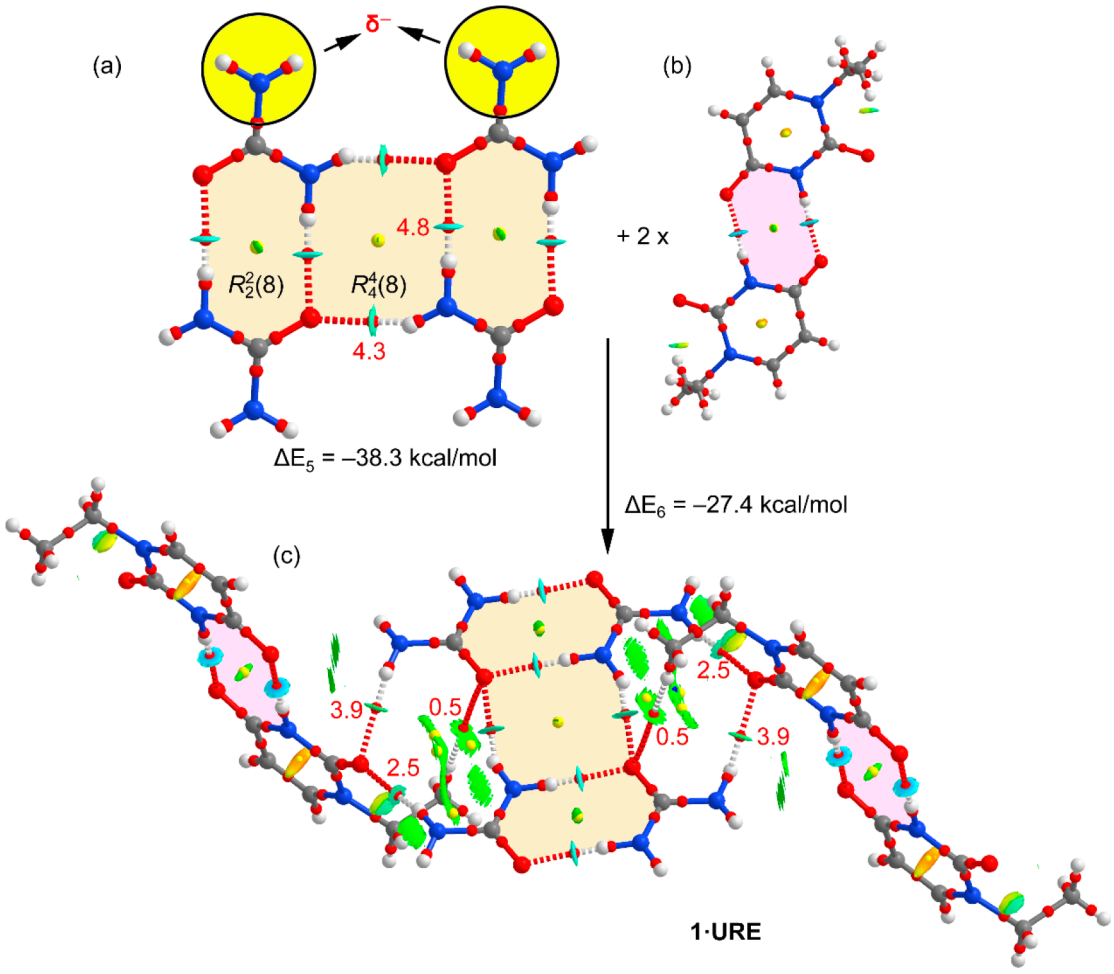

Figure 7. (a) QTAIM distribution of bond and ring CPs (red and yellow spheres, respectively) and NCIplot of the urea tetramer retrieved from the X-ray structure of **1·URE**. (b) QTAIM distribution of bond and ring CPs (red and yellow spheres, respectively) and NCIplot of the $R_2^2(8)$ dimer of **1·URE**. (c) QTAIM distribution of bond and ring CPs (red and yellow spheres, respectively) and NCIplot of the hexamer of compound **1·URE**, where the dissociation energies of the H-bonds derived from the G_r values are indicated in red (in kcal/mol). The formation energies (ΔE) computed at the PBE1PBE-D3/def2-TZVP level of theory are also indicated.

N groups (see Figure 5b). The C−H···O bonds are significantly weaker (1.9 and 1.6 kcal/mol), also in agreement with the NCIplot that shows green isosurfaces between the O and H atoms. Finally, the typical $R_2^2(8)$ motifs are formed between the carboxylic groups (see Figure 5c) in the solid state of this cocrystal. These H-bonds are very strong (9.8 kcal/mol), thus explaining the formation of the **4HB** homodimers in the crystal packing of **1·4HB_FII**.

Figure 6a shows the pentameric assembly present in the X-ray structure of **1·TAR**, where the central tartaric acid is surrounded by four uracil moieties. The QTAIM analysis reveals an intricate combination of H-bonds, where up to 12 H···O contacts are established. The formation energy of this assembly is very large (ΔE_3 = −41.7 kcal/mol) and is comparable to the sum of the individual dissociation energies, thus confirming that this assembly is governed by O−H···O and C−H···O contacts and also indicating the reliability of the QTAIM method in estimating the H-bond energies. It should be emphasized that, in contrast to the rest of the cocrystals, the uracil ring in **1·TAR** does not form the self-assembled $R_2^2(8)$ recurring motif. Instead, it forms strong C−O···H−O H-bonds where the most basic O4 atom and the most acidic H atoms of carboxylate groups interact. This agrees well with the information extracted by the QTAIM and NCIplot methods. That is, the dissociation energies are large (8.7 and 9.4 kcal/mol) and the NCIPlot isosurfaces that characterize these H-bonds are dark blue. The N−H···O H-bonds are weaker (4.3 and 4.4 kcal/mol, light blue NCIPlot isosurfaces) and similar to the O−H···O H-bonds involving the hydroxyl group of the tartaric acid (4.5 and 4.6 kcal/mol; latter value from Figure 6b). The ancillary C−H···O H-bonds are significantly weaker, ranging from 0.6 to 0.9 kcal/mol. The pentameric assembly represented in Figure 6a shows that there is one remaining hydroxyl group that is available for establishing additional interactions. In Figure 6b we show the H-bond formed by this remaining hydroxyl group with the adjacent uracil moiety in the X-ray structure. The combined QTAIM and NCIplot analyses show that, in addition to the O−H···O H-bond, several van der Waals and C−H···O contacts are also established, which are characterized by the green isosurfaces located between both monomers. The resulting interaction energy of this dimer is ΔE_4 = −9.0 kcal/mol, which is larger in absolute value than the sum of the dissociation energies of all H-bonds (6.3 kcal/mol) due to these additional van der Waals contacts.

Figure 7a shows a tetrameric fragment retrieved from the infinite 1D tape formed by the urea molecules in the solid state of **1·URE** (see also Figure 2a). The tape is formed by successive $R_2^2(8)$ and $R_4^4(8)$ synthons, where the carbonyl group of each

https://doi.org/10.1021/acs.cgd.1c00175
Cryst. Growth Des. 2021, 21, 4857−4870

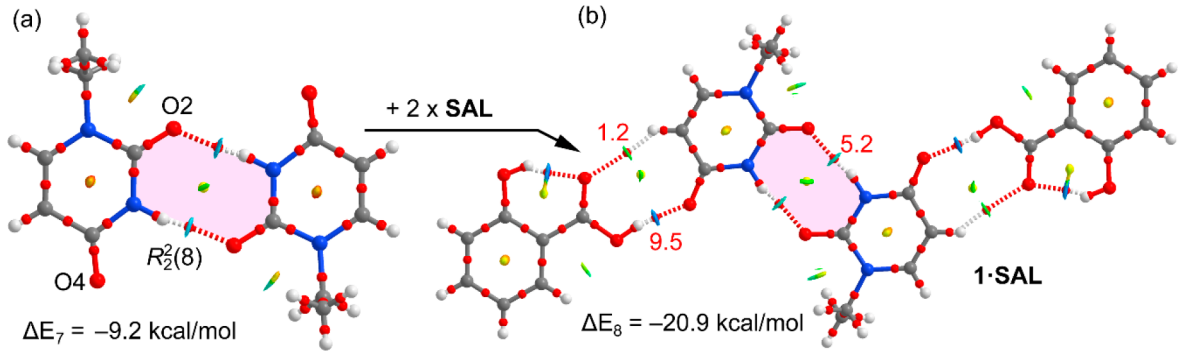

Figure 8. (a) QTAIM distribution of bond and ring CPs (red and yellow spheres, respectively) and NCIplot of the $R_2^2(8)$ dimer of **1·SAL**. (b) QTAIM distribution of bond and ring CPs (red and yellow spheres, respectively) and NCIplot of the tetramer of compound **1·SAL**, where the dissociation energies of the H-bonds derived from the G_r values are indicated in red (in kcal/mol). The formation energies (ΔE) computed at the PBE1PBE-D3/def2-TZVP level of theory are also indicated.

urea establishes two N–H···O bonds with the neighboring molecules. The formation energy of this tetramer is $\Delta E_5 = -38.3$ kcal/mol, which is larger than the sum of the dissociation energies of all H-bonds (27.8 kcal/mol), likely indicating the existence of favorable cooperativity effects. This interesting tetrameric assembly causes the NH_2 groups (two of them are highlighted in Figure 7a by yellow circles) to point toward the exterior of the tape, thus creating a region adequate for interacting with electron-rich atoms. In the solid state of **1·URE**, the uracil ring self-assembles via double N–H···O H-bonds ($R_2^2(8)$ motif), forming dimers similar to those described for **1·4HB_FII** (see Figure 5). This motif interacts with the urea tape by means of the available O2 atom that establishes a bifurcated H-bond with two NH_2 groups, as confirmed by the QTAIM analysis and the corresponding bond CPs and bond paths. A hexameric model of the cocrystal is represented in Figure 7c, where the interaction energy of the tetrameric urea assembly with two $R_2^2(8)$ dimers is $\Delta E_6 = -27.4$ kcal/mol.

In contrast to **1·4HB_FII**, **1·SAL** presents a self-assembled $R_2^2(8)$ dimer in the solid state, where O2 instead of O4 participates in the N–H···O H-bonds (see Figure 8a). The dimerization energy ($\Delta E_7 = -9.4$ kcal/mol) is smaller (in absolute value) than that of the $R_2^2(8)$ dimer of **1·4HB_FII** due to the participation of the less basic O2 atom. However, this allows the most basic O atoms to form strong H-bonds with the most acidic H atoms of the adjacent **SAL** molecules, thus forming the tetrameric assembly shown in Figure 8b. The formation energy of the tetramer considering the self-assembled $R_2^2(8)$ dimer previously formed is $\Delta E_8 = -20.9$ kcal/mol, which is similar in absolute value to the sum of the dissociation energies of the H-bonds (21.4 kcal/mol). The O–H···O H-bond is characterized by the corresponding bond CP and bond path and also a dark blue isosurface, in agreement with the large dissociation energy (9.5 kcal/mol) of this H-bond. It is interesting to highlight that the dissociation energy of this strong H-bond is slightly smaller than that computed for the homodimer of **4HB** in the **1·4HB_FII** cocrystal (9.8 kcal/mol; see Figure 5). However, **1·SAL** does not form carboxylic acid homodimers likely due to the existence of the ancillary C–H···O H-bonds (1.2 kcal/mol, see Figure 8b) that largely compensates for the small energetic difference between the O–H···O4 dissociation energy in **1·SAL** with respect to the O–H···O dissociation energy in the COOH···COOH homodimer in the **1·4HB** cocrystal.

CONCLUSIONS

In this study eight cocrystals with the modified nucleobase 1-ethyluracil and different types of coformers (urea and carboxylic acid derivatives) were successfully synthesized and characterized by powder X-ray diffraction, FT-IR spectroscopy, and TGA-DSC analysis. The crystal structures for six of them and a new hydrate of the coformer 4-hydroxybenzoic acid have been determined from single-crystal X-ray diffraction. Only for half of these six solved cocrystals was self-assembly between uracil units forming $R_2^2(8)$ uracil dimers observed, while for the other compounds (**1·MAL**, **1·TAR**, and **1·DHB**), the main interactions are established through hydrogen bonds with the coformer. Moreover, the cocrystals containing the dicarboxylic linear coformers L-malic and L-tartaric acids are isostructural and isomorphous, as deduced by a comparison of the PXRD patterns and unit cells.

The interactions were studied through DFT calculations, and in general, the behavior of the cocrystals reported herein agrees well with the MEP surface analysis, since in **1·TAR** and **1·SAL** the most basic O4 atom interacts with the acidic protons. Moreover, in **1·4HB** two different $R_2^2(8)$ homodimers are formed, one involving uracil and the other the carboxylic groups of the **4HB** coformer. It is also interesting to note the solid-state architecture of **1·URE** cocrystal, where the infinite 1D tape situates the NH_2 groups pointing to the exterior of the tape, allowing the $R_2^2(8)$ dimers to be accommodated via the formation of bifurcated H-bonds with the available O2 atom.

ASSOCIATED CONTENT

Supporting Information

The Supporting Information is available free of charge at https://pubs.acs.org/doi/10.1021/acs.cgd.1c00175.

Packing graphs of the crystal structure of 4-hydroxybenzoic acid monohydrate **4HB·H$_2$O**, FT-IR spectra, TGA-DSC thermograms of the new compounds, and hydrogen bond parameters for all the solved structures (PDF)

Accession Codes

CCDC 2059088–2059094 contain the supplementary crystallographic data for this paper. These data can be obtained free of charge via www.ccdc.cam.ac.uk/data_request/cif, or by emailing data_request@ccdc.cam.ac.uk, or by contacting The Cambridge Crystallographic Data Centre, 12 Union Road, Cambridge CB2 1EZ, UK; fax: +44 1223 336033.

https://doi.org/10.1021/acs.cgd.1c00175
Cryst. Growth Des. 2021, 21, 4857–4870

AUTHOR INFORMATION

Corresponding Authors

Antonio Frontera − *Departament de Química, Universitat de les Illes Balears, E-07122 Palma de Mallorca, Spain;* orcid.org/0000-0001-7840-2139; Email: toni.frontera@uib.es

Elies Molins − *Institut de Ciència de Materials de Barcelona (ICMAB-CSIC), 08193 Bellaterra, Spain;* orcid.org/0000-0003-1012-0551; Email: elies.molins@icmab.es

Authors

Yannick Roselló − *Departament de Química, Universitat de les Illes Balears, E-07122 Palma de Mallorca, Spain*

Mónica Benito − *Institut de Ciència de Materials de Barcelona (ICMAB-CSIC), 08193 Bellaterra, Spain*

Miquel Barceló-Oliver − *Departament de Química, Universitat de les Illes Balears, E-07122 Palma de Mallorca, Spain*

Complete contact information is available at: https://pubs.acs.org/10.1021/acs.cgd.1c00175

Author Contributions

The manuscript was written through contributions of all authors. All authors have given approval to the final version of the manuscript.

Notes

The authors declare no competing financial interest.

ACKNOWLEDGMENTS

This work has been carried out through MINECO/FEDER grant ENE2015-63969. M.B. and E.M. are grateful to the Severo Ochoa FunFuture project (MICINN, CEX2019-917S) and the Generalitat de Catalunya (2017SGR1687). M.B.-O. thanks the Vice-Rector for Research and International Relations of the University of the Balearic Islands for financial support in setting up the single-crystal X-ray diffraction facility. A.F. thanks the MICIU/AEI from Spain for financial support (Project CTQ2017-85821-R, Feder funds).

REFERENCES

(1) Desiraju, G. R. Crystal Engineering: from Molecule to Crystal. *J. Am. Chem. Soc.* **2013**, *135*, 9952−9967.

(2) Grepioni, F.; Braga, D. *Making Crystals by Design − from Molecules to Molecular Materials, Methods, Techniques, Applications*; Wiley-VCH: 2007; pp 209−240.

(3) Zhang, C.; Jiao, F.; Li, H. Crystal Engineering for Creating Low Sensitivity and Highly Energetic Materials. *Cryst. Growth Des.* **2018**, *18*, 5713−5726.

(4) Huang, C.; Xu, J.; Tian, X.; Liu, J.; Pan, L.; Yang, Z. High-Yielding and Continuous Fabrication of Nanosized CL-20-Based Energetic Cocrystals via Electrospraying Deposition. *Cryst. Growth Des.* **2018**, *18*, 2121−2128.

(5) Elder, D. P.; Holm, R.; Lopez de Diego, H. Use of pharmaceutical salts and cocrystals to address the issue of poor solubility. *Int. J. Pharm.* **2013**, *453*, 88−100.

(6) Dai, X.-L.; Li, S.; Chen, J.-M.; Lu, T.-B. Improving the Membrane Permeability of 5-Fluorouracil via Cocrystallization. *Cryst. Growth Des.* **2016**, *16*, 4430.

(7) Roselló, Y.; Benito, M.; Molins, E.; Barceló-Oliver, M.; Frontera, M. Adenine as a Halogen Bond Acceptor: A Combined Experimental and DFT Study. *Crystals* **2019**, *9*, 224.

(8) Choquesillo-Lazarte, D.; Nemec, V.; Cincic, D. Halogen bonded cocrystals of active pharmaceutical ingredients: pyrazinamide, lidocaine and pentoxifylline in combination with haloperfluorinated compounds. *CrystEngComm* **2017**, *19*, 5293.

(9) Makhotkina, O.; Lieffrig, J.; Jeanning, O.; Fourmigué, M.; Aubert, E.; Espinosa, E. Cocrystal or Salt: Solid State-Controlled Iodine Shift in Crystalline Halogen-Bonded Systems. *Cryst. Growth Des.* **2015**, *15*, 3464−3473.

(10) Baldrighi, M.; Bartesaghi, D.; Cavallo, G.; Chierotti, M. R.; Gobetto, R.; Metrangolo, P.; Pilati, T.; Resnati, G.; Terraneo, G. Polymorphs and co-crystals of haloprogin: an antifungal agent. *CrystEngComm* **2014**, *16*, 5897.

(11) Kavanagh, O. N.; Croker, D. M.; Walker, G. M.; Zaworotko, M. J. Pharmaceutical cocrystals: from serendipity to design to application. *Drug Discovery Today* **2019**, *24*, 796−804.

(12) Koch, E. S.; McKenna, K. A.; Kim, H. J.; Young, V. G.; Swift, J. A. Thymine cocrystals based on DNA-inspired binding motifs. *CrystEngComm* **2017**, *19*, 5679−5685.

(13) Thomson, J. M.; Lamont, I. L. Nucleoside analogues as antibacterial agents. *Front. Microbiol.* **2019**, *10*, 952.

(14) Bardagí, J. I.; Rossi, R. A. Advances in the synthesis of 5- and 6-Substituted Uracil Derivatives. *Org. Prep. Proced. Int.* **2009**, *41*, 479−514.

(15) Chakraborty, S.; Ganguly, S.; Desiraju, G. R. Synthon transferability probed with IR spectroscopy: cytosine salts as models for salts of lamivudine. *CrystEngComm* **2014**, *16*, 4732−4741.

(16) de la Torre, B. G.; Albericio, F. The Pharmaceutical Industry in 2019. An Analysis of FDA Drug Approvals from the Perspective of Molecules. *Molecules* **2020**, *25*, 745.

(17) Venturini, M. Rational Development of Capecitabine. *Eur. J. Cancer* **2002**, *38*, 3−9.

(18) Pedireddi, V. R.; Ranganathan, A.; Ganesh, K. N. Cyanurate Mimics of Hydrogen-bonding patterns of Nucleic Bases: Crystal Structure of a 1:1 Molecular Complex of 9-Ethyladenine and N-Methylcyanuric Acid. *Org. Lett.* **2001**, *3*, 99−102.

(19) Portalone, G.; Colapietro, M. The 1:1 complex of cytosine and 5-fluorouracil monohydrate revisited. *Acta Crystallogr., Sect. C: Cryst. Struct. Commun.* **2007**, *63*, o423−o425.

(20) Barnett, S. A.; Hulme, A. T.; Tocher, D. A. 5-Fluorouracil and thymine form a crystalline solution. *Acta Crystallogr., Sect. C: Cryst. Struct. Commun.* **2006**, *C62*, No. o412.

(21) Kim, S.-H.; Rich, A. A non-complementary hydrogen-bonded complex containing 5-fluorouracil and 1-methylcytosine. *J. Mol. Biol.* **1969**, *42*, 87−95.

(22) Gerhardt, V.; Egert, E. Cocrystals of 6-chlorouracil and 6-chloro-3-methyluracil: explorin their hydrogen-bond-based synthon motifs with several triazine and pyrimidine derivatives. *Acta Crystallogr., Sect. B: Struct. Sci., Cryst. Eng. Mater.* **2015**, *B71*, 209−220.

(23) Hutzler, W. M.; Egert, E. Cocrystals of 6-methyl-2-thiouracil: presence of the acceptor-donor-acceptor/donor-acceptor-donor synthon. *Acta Crystallogr., Sect. C: Struct. Chem.* **2015**, *C71*, 229−238.

(24) Kumar, V.; Goswami, P. K.; Thaimattam, R.; Ramanam, A. Multicomponent solids of uracil derivatives, orotic and isoorotic acids. *CrystEngComm* **2018**, *20*, 3490−3504.

(25) Mohana, M.; Muthiah, P. T.; McMillen, C. D. Supramolecular hydrogen-bonding patterns in 1:1 cocrystals of 5-fluorouracil with 4-methylbenzoic acid and 3-nitrobenzoic acid. *Acta Crystallogr., Sect. C: Struct. Chem.* **2017**, *C73*, 259−263.

(26) Delori, A.; Eddleston, M. D.; Jones, W. Cocrystals of 5-fluorouracil. *CrystEngComm* **2013**, *15*, 73−77.

(27) Zaitu, S.; Miwa, Y.; Taga, T. A 2:1 molecular complex of theophylline and 5-Fluorouracil as the Monohydrate. *Acta Crystallogr., Sect. C: Cryst. Struct. Commun.* **1995**, *C51*, 1857−1859.

(28) Li, S.; Chen, J.-M.; Lu, T.-B. Synthon polymorphs of 1−1 co-crystal of 5-fluorouracil and 4-hydroxybenzoic acid: their relative stability and solvent polarity dependence of grinding outcomes. *CrystEngComm* **2014**, *16*, 6450−6458.

(29) Moisescu-Goia, C.; Muresan-Pop, M.; Simon, V. New solid-state forms of antineoplastic 5-fluorouracil with anthelmintic piperazine. *J. Mol. Struct.* **2017**, *1150*, 37−43.

(30) Enkelmann, D. D.; Handelmann, J.; Schauerte, C.; Merz, K. Co-crystallization and polymorphic behaviour of 5-fluorouracil. *CrystEngComm* **2019**, *21*, 2130−2134.

(31) Dai, X.-L.; Voronin, A. P.; Huang, Y.-L.; Perlovich, G. L.; Zhao, X.-H.; Lu, T.-B.; Chen, J.-M. 5-Fluorouracil cocrystals with lipophilic hydroxyl-2-naphthoic acids: crystal structures, theoretical computations, and permeation studies. *Cryst. Growth Des.* **2020**, *20*, 923−933.
(32) Aitipamula, S.; Chow, P. S.; Tan, R. B. H. Crystal Engineering of Tegafur Cocrystal: Structural Analysis and Physicochemical Properties. *Cryst. Growth Des.* **2014**, *14*, 6557−6569.
(33) https://www.fda.gov/food/ingredientspackaginglabeling/gras/ or https://www.fda.gov/Food/IngredientsPackagingLabeling/FoodAdditivesIngredients/ucm115326.htm.
(34) Nechipadappu, S. K.; Reddy, I. R.; Tarafder, K.; Trivedi, D. R. Salt/Cocrystal of anti-fibrinolytic chemostatic drug tranexamic acid: structural, DFT, and stability study of salt/cocrystal with GRAS molecules. *Cryst. Growth Des.* **2019**, *19*, 347−361.
(35) Barceló-Oliver, M. Interaccions entre ions metàl·lics i composts d'interès biològic (halouracils i derivats sintètics, hipurats i aciclovir). Interaccions mètal·liques que desenvolupen noves molècules anticanceroses; Tesi Doctoral; Universitat de les Illes Balears, 2009.
(36) Farrugia, L. J. WinGX suite for small-molecule single-crystal crystallography. *J. Appl. Crystallogr.* **1999**, *32*, 837−838.
(37) Sheldrick, G. M. Crystal structure refinement with SHELXL. *Acta Crystallogr., Sect. A: Found. Adv.* **2015**, *71*, 3−8.
(38) Burla, M. C.; Caliandro, R.; Carrozzini, B.; Cascarano, G. L.; Cuocci, C.; Giacovazzo, C.; Mallamo, M.; Mazzone, A.; Polidori, G. Crystal structure determination and refinement via SIR2014. *J. Appl. Crystallogr.* **2015**, *48*, 306−309.
(39) Blessing, R. H. An empirical correction for absorption anisotropy. *Acta Crystallogr., Sect. A: Found. Crystallogr.* **1995**, *A51*, 33−38.
(40) *SADABS, Ver. 1*; Bruker-AXS Inc.: 2004.
(41) Sheldrick, G. M. SHELXT - Integrated space-group and crystal-structure determination. *Acta Crystallogr., Sect. A: Found. Adv.* **2015**, *A71*, 3−8.
(42) Dolomanov, O. V.; Bourhis, L. J.; Gildea, R. J.; Howard, J. A. K.; Puschmann, H. *J. Appl. Crystallogr.* **2009**, *42*, 339−241.
(43) Spek, A. L. Single-crystal structure validation with the program PLATON. *J. Appl. Crystallogr.* **2003**, *36* (1), 7−13.
(44) Frisch, M. J.; Trucks, G. W.; Schlegel, H. B.; Scuseria, G. E.; Robb, M. A.; Cheeseman, J. R.; Scalmani, G.; Barone, V.; Petersson, G. A.; Nakatsuji, H.; Li, X.; Caricato, M.; Marenich, A. V.; Bloino, J.; Janesko, B. G.; Gomperts, R.; Mennucci, B.; Hratchian, H. P.; Ortiz, J. V.; Izmaylov, A. F.; Sonnenberg, J. L.; Williams-Young, D.; Ding, F.; Lipparini, F.; Egidi, F.; Goings, J.; Peng, B.; Petrone, A.; Henderson, T.; Ranasinghe, D.; Zakrzewski, V. G.; Gao, J.; Rega, N.; Zheng, G.; Liang, W.; Hada, M.; Ehara, M.; Toyota, K.; Fukuda, R.; Hasegawa, J.; Ishida, M.; Nakajima, T.; Honda, Y.; Kitao, O.; Nakai, H.; Vreven, T.; Throssell, K.; Montgomery, J. A., Jr.; Peralta, J. E.; Ogliaro, F.; Bearpark, M. J.; Heyd, J. J.; Brothers, E. N.; Kudin, K. N.; Staroverov, V. N.; Keith, T. A.; Kobayashi, R.; Normand, J.; Raghavachari, K.; Rendell, A. P.; Burant, J. C.; Iyengar, S. S.; Tomasi, J.; Cossi, M.; Millam, J. M.; Klene, M.; Adamo, C.; Cammi, R.; Ochterski, J. W.; Martin, R. L.; Morokuma, K.; Farkas, O.; Foresman, J. B.; Fox, D. J. *Gaussian 16, Rev. A.01*; Gaussian, Inc.: 2016.
(45) Adamo, C.; Barone, V. Toward reliable density functional methods without adjustable parameters: The PBE0 model. *J. Chem. Phys.* **1999**, *110*, 6158−69.
(46) Rozhkov, A.; Eliseeva, A. A.; Baykov, S. V.; Galmés, B.; Frontera, A.; Kukushkin, V. Y. One-Pot Route to X-perfluoroarenes (X = Br, I) Based on FeIII-Assisted C−F Functionalization and Utilization of These Arenes as Building Blocks for Crystal Engineering Involving Halogen Bonding. *Cryst. Growth Des.* **2020**, *20*, 5908−5921.
(47) Álvarez-Vidaurre, R.; Castiñeiras, A.; Frontera, A.; García-Santos, I.; Gil, D. M.; González-Pérez, J. M.; Niclós-Gutiérrez, J.; Torres-Iglesias, R. Weak Interactions in Cocrystals of Isoniazid with Glycolic and Mandelic Acids. *Crystals* **2021**, *11* (4), 328.
(48) Verdugo-Escamilla, C.; Alarcon-Payer, C.; Frontera, A.; Acebedo-Martínez, F. J.; Domínguez-Martín, A.; Gómez-Morales, J.; Choquesillo-Lazarate, D. Interconvertible hydrochlorothiazide-caffeine multicomponent pharmaceutical materials: a solvent issue. *Crystals* **2020**, *10* (12), 1088.
(49) Boys, S. F.; Bernardi, F. The calculation of small molecular interactions by the differences of separate total energies. Some procedures with reduced errors. *Mol. Phys.* **1970**, *19*, 553−566.
(50) Keith, T. A. *AIMAll, Ver. 13.05.06*; TK Gristmill Software: 2013.
(51) https://dictionary.iucr.org/Isostructural_crystals.
(52) Tarai, A.; Baruah, J. B. Quaternary and senary sub-assemblies in cocrystals and salts of quinoline-4-carbaldoxime with aromatic carboxylic acids. *CrystEngComm* **2016**, *18*, 9095−9102.
(53) Galcera, J.; Molins, E. Effect of the Counterion on the Solubility of Isostructural Pharmaceutical Lamotrigine Salts. *Cryst. Growth Des.* **2009**, *9*, 327−334.
(54) Oliveira, M. A.; Peterson, M. L.; Klein, D. Continuously Substituted Solid Solutions of Organic Co-Crystals. *Cryst. Growth Des.* **2008**, *8*, 4487−4493.
(55) Bombicz, P.; May, N. V.; Fegyverneki, D.; Saranchimeg, A.; Bereczki, L. Methods for easy recognition of isostructurality − lab jack-like crystal structures of halogenated 2-phenylbenzimidazoles. *CrystEngComm* **2020**, *22*, 7193−7203.
(56) Luo, Y.-H.; Xu, B.; Sun, B.-W. Investigation of supramolecular synthons of p-hydroxybenzoic acid (PHBA): Comparison of its hydrate, co-crystal and salt. *J. Cryst. Growth* **2013**, *374*, 88−98.
(57) Gobira Lopes, L.; Lopes Tavares, G.; Dias Thomaz, L.; Sabino, J. R.; Borges, K.; Vieira, P. C.; Moura Veiga, T. A.; de Souza Borges, W. Taraxerol 4-methoxybenzoate, an in vitro of photosynthesis isolated from Pavonia multiflora A. ST-HIL. (Malvaceae). *Chem. Biodiversity* **2016**, *13*, 284−292.
(58) Fukuyama, K.; Ohkura, K.; Kashino, S.; Haisa, M. The crystal and molecular structure of p-Hydroxybenzoic acid monohydrate. *Bull. Chem. Soc. Jpn.* **1973**, *46* (3), 804−808.
(59) Braun, D. E.; Karamertzani, P. G.; Arlin, J.-B.; Florence, A. J.; Kahlenberg, V.; Tocher, D. A.; Griesser, U. J.; Price, S. L. Solid-state of S-resorcylic acid: how exhaustive should a polymorph screen be? *Cryst. Growth Des.* **2011**, *11* (1), 210−220.
(60) Vener, M. V.; Egorova, A. N.; Churakov, A. V.; Tsirelson, V. G. Intermolecular hydrogen bond energies in crystals evaluated using electron density properties: DFT computations with periodic boundary conditions. *J. Comput. Chem.* **2012**, *33*, 2303−2309.
(61) Espinosa, E.; Lecomte, C.; Molins, E. Experimental electron-ndensity overlapping in hydrogen bonds: topology vs. energetics. *Chem. Phys. Lett.* **1999**, *300*, 745−748.
(62) Espinosa, E.; Alkorta, I.; Elguero, J.; Molins, E. From weak to strong interactions: A comprehensive analysis of the topological and energetic properties of the electron density distribution involving XH···FY systems. *J. Chem. Phys.* **2002**, *117*, 5529−5542.

NOTE ADDED AFTER ASAP PUBLICATION

The spelling of the author name Roselló was corrected on August 5, 2021.

https://doi.org/10.1021/acs.cgd.1c00175
Cryst. Growth Des. 2021, 21, 4857−4870